

# The Production of Polycyclic Aromatic Hydrocarbon Anions in Inert Gas Matrices Doped with Alkali Metals. Electronic Absorption Spectra of the Pentacene Anion ( $C_{22}H_{14}^-$ ).

Thomas M. Halasinski, Douglas M. Hudgins, Farid Salama, and Louis J. Allamandola

*NASA Ames Research Center, Mail Stop: 245-6, Moffett Field, CA 94035-1000*

## ABSTRACT

The absorption spectra of pentacene ( $C_{22}H_{14}$ ) and its radical cation ( $C_{22}H_{14}^+$ ) and anion ( $C_{22}H_{14}^-$ ) isolated in inert-gas matrices of Ne, Ar, and Kr are reported from the ultraviolet to the near-infrared. The associated vibronic band systems and their spectroscopic assignments are discussed together with the physical and chemical conditions governing ion (and counterion) production in the solid matrix. In particular, the formation of isolated pentacene anions is found to be optimized in matrices doped with alkali metal (Na and K).

## 1. INTRODUCTION

The detection and unambiguous characterization of transient molecular species within the interstellar medium (ISM) require laboratory spectroscopic investigations of individual species under relevant conditions. Through the conjunction of astronomical observations and laboratory astrophysical experiments, the number of positive detections of known molecular species in the ISM has been increasing from the first molecule detected in 1937, methylidyne (CH) through one of its electronic absorption bands,<sup>1</sup> to more recent detections of molecules as large as HC<sub>11</sub>N using radio emission spectroscopy.<sup>2</sup> Charged molecular species have also been found within the ISM.<sup>3</sup>

Ionic species are important in the chemical reaction schemes which control the variety and abundance of molecules found within interstellar molecular clouds which are comprised of both dust and gaseous material. These molecular clouds can eventually condense to form stars, and, ultimately, stars contribute material back to the ISM during the last stages of their lifecycle. Thus, knowledge of the chemical identity of the species within molecular clouds is crucial to the overall understanding of the evolution of the ISM.

While it has proved difficult to unambiguously identify individual molecular species responsible for a distinctive family of infrared emission features observed from matter at all stages of the lifecycle of the ISM, there is now strong evidence that these ubiquitous emission features arise from carbonaceous aromatic materials and, in particular, from neutral and ionized polycyclic aromatic hydrocarbons (PAHs).<sup>4-6</sup> PAHs are also thought to contribute to the diffuse interstellar bands (DIBs) seen in absorption in the optical spectra of stars that are obscured by diffuse interstellar clouds.<sup>7,8</sup> Furthermore, in recent years, it has been shown that several of the observed vibronic transitions of PAH cations match up well with known DIBs.<sup>8</sup> In both the infrared emission and DIB cases, PAHs are considered good candidates because they are stable against ultraviolet photodissociation, a requirement to maintain the concentration necessary in the ISM where materials are exposed to harsh far-UV radiation fields.

Negatively-charged PAHs are also expected to play an important role in the evolution of interstellar clouds.<sup>7,9-15</sup> It has been postulated that PAH anions constitute the dominant negative charge carrier inside dense molecular clouds, and as such regulate the charge balance in these

regions.<sup>9-15</sup> This, in turn, influences the molecular complexity found in the interstellar environment through ion-molecule reactions. Photodetachment of PAH anions provide a significant heat source in interstellar clouds, affecting the chemical reaction rates of the molecular species within the cloud, and ultimately the thermal stability and structure of the cloud itself.<sup>11</sup>

Although anionic PAHs may be an important component in the interstellar medium, the spectroscopy of negatively-charged PAHs in an astrophysically relevant environment has been largely unexplored. Electronic spectra of several PAH anions have been previously studied in glassy organic solids.<sup>16,17</sup> This environment induces strong perturbations on the energy levels of the trapped ions, making comparisons to astronomical data difficult, if not impossible. Matrix-isolation spectroscopy, however, is the dominant method for the study of isolated ions and is an especially well suited technique for the simulation of the low temperature and low molecular density interstellar environments.<sup>18</sup> However, an extensive survey of the electronic spectroscopy of PAH ions in rare gas matrices has shown that, with the notable exception of pentacene,<sup>19</sup> no spectroscopic signatures associated with PAH anions have been reported thus far. This may be an indication of the relatively weak bonding or strong repulsive character of the potential curves associated with the higher excited electronic states of the PAH anions. The relatively high electron affinity of pentacene (1.35 eV)<sup>20</sup> may explain the observation of spectral features of the pentacene anion in an Ar matrix.<sup>19,21</sup>

A particularly successful method of producing molecular anions in rare gas matrices has been developed by Kasai<sup>22,23</sup> for electron spin resonance spectroscopy studies. In this method, Na atoms are used as matrix dopants. Upon photoexcitation of the matrix with suitable radiation, the metal atoms act as electron donors, which leads to the formation of anions of the molecular guest. This report describes experimental studies in which we have co-deposited the PAH pentacene ( $C_{22}H_{14}$ ) with an alkali metal (Na or K) in Ne, Ar and Kr matrices, photoionized the matrix, and probed the matrices spectroscopically from the ultraviolet (180 nm) to the infrared ( $500\text{ cm}^{-1}$ ). Given its relatively high electron affinity and the availability of spectroscopic data on its anion, pentacene represents the ideal prototype to explore and optimize the use of alkali metal dopants in rare gas matrices to facilitate the production of matrix-isolated PAH anions.

## 2. EXPERIMENTAL

The experimental instrumentation used in the matrix-isolation studies reported here has been previously described in detail. Two independent instruments were employed in these studies, a UV/visible/near-IR spectrometer<sup>24, 25</sup> and an FTIR spectrometer,<sup>26, 27</sup> each equipped with its own dedicated sample vacuum chamber and matrix deposition source. A brief review will be given here of the procedures followed in preparation of the sample matrix, along with a more detailed description of the modifications used to co-deposit alkali metal vapor along with pentacene vapor.

The UV/visible/near-IR instrument is equipped with a sapphire sample window cooled to 4.2 K by an extended liquid helium transfer cryostat, while the FTIR instrument uses a CsI window cooled to 10 K by a closed-cycle helium refrigerator. Both sample windows can be rotated 360° under vacuum to face, alternatively, two spectroscopic window ports, the matrix gas and PAH/alkali metal vaporization lines, and a MgF<sub>2</sub> vacuum-UV window port.

Single beam spectra of the cold substrate were collected before the matrix was deposited and used as the background for all spectra reported unless noted otherwise. On the UV/visible/near-IR instrument, a deuterium lamp provides spectral output from 160-360 nm and a quartz tungsten halogen lamp provides output from 320-2500 nm. The FTIR instrument employs a Globar for the mid-IR and a tungsten lamp for the near-IR. A Corning 2-60 filter was placed in front of the tungsten lamp of the FTIR to limit the spectral output to wavelengths longer than 665 nm (~1.9 eV). Spectra were recorded from 180-1000 nm on the UV/visible/near-IR instrument with a nominal resolution of 0.1 nm. Spectra on the FTIR instrument were recorded from 15100-8800 cm<sup>-1</sup> (662-1136 nm) and 5000-500 cm<sup>-1</sup> with 0.5 cm<sup>-1</sup> resolution.

The vaporization and co-deposition of pentacene and the alkali metals was performed using Pyrex tubes (12.7 mm OD) which were mounted on the sample chamber through two stainless steel Cajon Ultratorr fittings and heated from outside the vacuum chamber with the use of heating tape. The tubes were positioned between 4 and 5 cm from the cold window and angled inward in such a way that the vapor exiting each tube coalesced immediately before the surface of the cold substrate. The temperature of each tube was monitored using a chromel/alumel thermocouple

mounted on the exterior of each tube with Al foil tape. Some experiments reported here also utilized two resistively heated stainless-steel tubes (5 mm dia) similar to that reported by Kasai<sup>22, 23</sup> to vaporize the pentacene and alkali metal samples. These tubes were positioned 3 cm from the surface of the cold substrate and resistively heated from within the sample window vacuum chamber. Both the Pyrex and stainless-steel tube vaporization apparatuses produced matrices of similar spectral quality.

Matrix gas was admitted through a port at a position 45° from the plane of the substrate surface and the median between the tubes containing pentacene and alkali metal such that the three vapor streams combined before the surface of the window. Typical deposition temperatures for pentacene, Na, and K on both vaporization apparatus were 175-225°C, 205-235°C, and 110-130°C, respectively. Ne flow rates were estimated to be 12 mmol/h while typical Ar flow rates were decreased to 0.5 mmol/h to reduce the light scattering of the matrix. Based on these flow rates and vaporization temperatures, the matrix/pentacene/alkali metal ratio is estimated to be in excess of 800/1/1. Typical deposition times varied from 2 to 4 hrs.

Three photolysis lamps were used in the experiments reported here. An OSRAM mercury arc lamp (HBO 100 W/2) operated by a PTI (LPS 200) power supply and filtered with a Pyrex and H<sub>2</sub>O filter produced radiation from 300-1200 nm (4.1-1.0 eV) with the maximum intensity at 2.1 eV. The output of the mercury lamp was directed through a quartz or MgF<sub>2</sub> spectroscopic window port to the cooled sapphire substrate during photolysis of the matrix. Experiments were also performed in which the full output of a standard Na arc lamp (George W. Gates & Co.) was used as a photolysis source (2.1 eV) in a similar manner as that of the mercury lamp. A microwave-powered, hydrogen flow (10% H<sub>2</sub>/He), discharge lamp (Ophos Instruments MPG 4M) mounted on the MgF<sub>2</sub> vacuum chamber window produced nearly monochromatic radiation in the Lyman  $\alpha$  line at 121.6 nm (10.2 eV). Typical photolysis times ranged from 2 to 20 minutes.

Pentacene (98+%) was obtained from Aldrich Chemical Co. and was used as received. Na chunks (98%) stored in mineral oil were obtained from Aldrich Chemical Co. Immediately prior to use, Na pieces (~3 mm<sup>3</sup>) were prepared by cleaving larger chunks to produce essentially clean and oil-free Na samples. K samples were prepared in a similar fashion. Ne (Cryogenic Rare Gas

99.9995%), Ar (Matheson 99.998%), and Kr (Cryogenic Rare Gas 99.995%) research grade rare gases were used without further purification.

### **3. RESULTS AND DISCUSSION**

A series of studies were performed to ascertain the feasibility of (i) producing PAH anions from neutral PAH precursors isolated in rare gas matrices doped with alkali metals and (ii) spectroscopically measuring their electronic absorption spectra. In these experiments, alkali metals were co-deposited with pentacene in rare gas matrices, and several experimental variables, such as vaporization temperatures, matrix gas flow rates, choice of matrix material, choice of alkali metal, photolysis energy and duration were explored. We report and discuss the spectra which illustrate the successful production of isolated pentacene anions in rare gas matrices and the optimal conditions for their production.

#### **3.1. Electronic spectroscopy of the alkali metals, Na and K, isolated in rare gas matrices**

Initial experiments focused on the spectra of isolated alkali metals (Na and K) in both Ar and Ne matrices to assist in the assignment of spectral features observed when the alkali metals were co-deposited with pentacene in a rare gas matrix. Depositions of Na into a growing rare gas matrix appeared orange to orange-red while depositions of K produced rare gas matrices which appeared blue in color. Figures 1A and 1B display the visible/near-IR spectra (370-1000 nm) measured with the UV/visible/near-IR spectrometer when Na is deposited in Ar and Ne matrices, respectively. Likewise, Figures 1C and 1D display the visible/near-IR spectra observed in the same region when K is deposited in Ar and Ne, respectively. Depositions of Na in the rare gas matrices exhibit a number of very strong and broad features in the visible range while depositions of K exhibit very strong and broad features in the visible/near-IR range. In both cases, no absorbance features are observed in the UV range up to the detection limit of the spectrometer (180 nm). The spectral structure is highly sensitive to experimental parameters such as the vaporization temperature of the alkali metal, the flow rate of the rare gas, and the temperature of the

matrix. These observations are in global agreement with previous studies<sup>28-43</sup> which show that alkali metals produce a number of broad spectral features in the visible/near-IR when trapped in rare gas matrices. We discuss the spectra of Figure 1 case by case below.

### 3.1.1. Na/Ar

The spectrum of Na/Ar (Figure 1A) shows a structured broad absorption band in the 400-750 nm region. The features in the 490-610 nm region are attributed to the  $D_1$  and  $D_2$  lines of the free Na atom which fall at 589.6 and 589.0 nm, respectively, and are associated with the  $3p$  ( $^2P_{1/2, 3/2}$ )  $\leftarrow$   $3s$  ( $^2S_{1/2}$ ) transitions. The observed structure of the spectrum, although less pronounced than in the case of K isolated in an Ar matrix (Figure 1C), is in agreement with the spectroscopy of Na isolated in Ar matrices discussed in the literature,<sup>28-34</sup> where the electronic states of Na are observed to be strongly perturbed by the solid matrix environment. We note, in particular, that the spectrum shown in Figure 1A is in good qualitative agreement with the spectra reported by Tam et al.<sup>31</sup> and Silverman et al.<sup>33</sup> as indicated by the formation of different trapping sites resulting in bands around 510, 550 and 580 nm in Figure 1A. Although it is not deconvolved in the spectrum displayed here, each trapping site can yield a multiplet absorption. The multiplet structure within each of the three bands is due to the breaking of the threefold degeneracy of the excited metal atom  $P$  state by the matrix environment and has been explained with a dynamic Jahn-Teller effect model.<sup>32</sup> The broad band at 460 nm has been assigned to another trapping site of atomic Na<sup>29</sup> and, alternatively, to the  $^1\Pi_u \leftarrow X^1\Sigma_g^+$  transition of Na<sub>2</sub>.<sup>34</sup> The latter assignment seems more probable, however, with regard to the fact that a broad band at 630 nm, which has been assigned to the  $^1\Sigma_u^+ \leftarrow X^1\Sigma_g^+$  transition of Na<sub>2</sub>,<sup>28</sup> is indeed observed.

### 3.1.2. Na/Ne

The spectrum of Na/Ne (Figure 1B) consists of a strong and very broad feature with two distinguishable peaks which fall around 450 and 500 nm, respectively. While, to our knowledge, spectra of Na in Ne are not available in the literature for comparison, Wright and Balling<sup>35</sup> have, however, reported the positions of two spectral features around 545 and 590 nm with a similar

lack of multiplets in their study of Na trapped in a 3 K Ne matrix. In the absence of any further experimental and theoretical studies, it is difficult to assess the causes of this discrepancy. It is tempting, however, to invoke the strong influence of the Ne matrix structure on the spectral features of the trapped Na to explain the differences seen between the two experiments. Furthermore, a survey of the results presented here together with the published literature<sup>31</sup> indicates that the matrix-induced perturbation in the spectrum of atomic Na increases when going from Xe to Kr to Ar to Ne. Perhaps this is indicative of a metal whose core electrons are isoelectronic with Ne and whose valence electron has some probability of diffusing into the Ne lattice. We tentatively associate the band around 500 nm with the  $3p (^2P_{1/2, 3/2}) \leftarrow 3s (^2S_{1/2})$  transitions of atomic Na. The band around 450 nm may be related to a transition within the dimer  $\text{Na}_2$ , analogous to the band observed at 460 nm in Ar.

### 3.1.3. K/Ar

The spectrum of K/Ar (Figure 1C) shows a number of broad absorption bands in the 400-900 nm region. The observed structure of the spectrum is in good agreement with the spectroscopy of matrix-isolated K discussed in the literature.<sup>36-43</sup> We note, in particular, that the spectrum shown in Figure 1C is in good qualitative agreement with the spectra reported in references 40, 42, and 43. The bands in the 720-800 nm region are close to the  $D_1$  and  $D_2$  lines of the free K atom which fall at 769.9 and 766.5 nm, respectively, and are associated with the  $4p (^2P_{1/2, 3/2}) \leftarrow 4s (^2S_{1/2})$  transitions. The bands in the 640-720 nm are associated with the trapping of atomic K in a different site in the matrix.<sup>39-43</sup> Annealing studies<sup>40, 43</sup> seem to indicate that atomic K is more stable in this second trapping site. A triplet structure within each trapping site observed in previous reports has been explained by a dynamic Jahn-Teller effect in the excited p state,<sup>40, 41, 43</sup> similar to the case of Na isolated in Ar matrices. The other, weaker, bands seen in the spectrum can be attributed to K dimers (for the 870 and 580 nm bands) and higher order clusters (for the bands around 540 and 510 nm) in agreement with previous observations.<sup>40, 43</sup> The relatively strong band at 870 nm has been attributed to the  $^1\Sigma_u^+ \leftarrow ^1\Sigma_g^+$  transition of  $\text{K}_2$ .<sup>40</sup>

#### 3.1.4. K/Ne

The spectrum of K/Ne (Figure 1D), too, shows a number of broad absorption bands in the 400-900 nm region. No data is available in the literature for comparison as far as the authors are aware. However, by comparison with the spectra in Ar matrices,<sup>36-43</sup> we tentatively relate the bands in the 710-810 nm and 580-710 nm regions, respectively, with the  $4p$  ( $^2P_{1/2, 3/2}$ )  $\leftarrow$   $4s$  ( $^2S_{1/2}$ ) transitions of atomic K trapped in different matrix sites. The other bands can be similarly attributed to dimers and higher clusters of atomic K. We note that the strong dimer ( $K_2$ ) absorption band is blue-shifted to 850 nm as compared with the Ar matrix at 870 nm.

### 3.2. Electronic spectroscopy of pentacene isolated in rare gas matrices

The electronic spectrum of neutral pentacene isolated in rare gas matrices (Ne, Ar, and Kr) exhibits 3 band systems in the 250-1000 nm spectral window (see Figure 2) associated with transitions to the  $S_1$  ( $^1B_{2u}^+$ ),  $S_2$  ( $^1B_{3u}^-$ ), and  $S_3$  ( $^1B_{3u}^+$ ) states. The positions of the bands are listed in Table I. Assignment of the vibronic origins is based on measurements in solution (*n*-heptane).<sup>44, 45</sup> To our knowledge, high-resolution, gas-phase measurements of neutral pentacene have been reported only for the first excited electronic state band origin at 536.2 nm.<sup>46</sup> This compares well with our measurement in a Ne matrix at 544.4 nm. The gas-phase to matrix shift ( $\nu_{(\text{gas-matrix})} / \nu_{\text{gas}}$ ) for this band origin corresponds to 1.5 %, 4.2 %, and 5.3 % respectively in Ne, Ar, and Kr. The increase in the matrix-induced shift indicates an increased interaction between the trapped pentacene molecule and the host matrix. This effect is expected from the increased polarization of the matrix material when going from Ne to Kr. The influence of the molecular size of the trapped molecule on the matrix-shift can be seen by comparing the fractional shift of 1.5 % for pentacene in Ne observed here to the 0.25 % shift reported for naphthalene in Ne.<sup>24</sup> As with the case of naphthalene (also of  $D_{2h}$  symmetry), the totally symmetric vibrational modes are expected to dominate the vibronic transitions of pentacene.<sup>24</sup> Using the measured Raman vibrational bands of pentacene<sup>47</sup> as a guide, we have made tentative assignments for each observed vibronic transition (see Table I).

### 3.3. Electronic and vibrational spectroscopy of pentacene isolated in alkali-metal doped rare gas matrices

Figure 1E displays the visible/near-IR absorption spectrum obtained after both Na and pentacene are co-deposited in a Ne matrix. Most of the broad underlying absorption observed in this spectrum corresponds to that observed when only Na is deposited in Ne matrices (Figure 1B). Absorption bands due to the transitions associated with the  $S_1 (^1B_{2u}^+) \leftarrow S_0 (^1A_{1g})$  band system of isolated neutral pentacene molecules (Figure 2 and Table I) are also observed. Additional spectral features are observed in the region between 620 nm and 870 nm which only appear when *both* pentacene and Na are present in the matrix. Features in the mid-IR which are also observed only when both Na and pentacene are present in a rare gas matrix are displayed in Figure 3A and discussed in more detail below. Co-deposition of K with pentacene in rare gas matrices also reveals spectral features in the visible/near-IR which are not present when only one of the species is trapped in the matrix.

Although the precise origin of these features remains in question, it is clear that they originate from a complex involving a pentacene molecule(s) and one or more alkali metal atoms. Furthermore, experiments in which the deposition temperature of pentacene and the alkali metal were varied produced changes in the relative band strengths in the infrared which are attributable to a complex, suggesting that more than one complex is formed during the matrix deposition. In the remaining discussion, we will refer to these uncharacterized species as an [alkali metal - pentacene] complex. Evidence is found for the simultaneous presence of isolated pentacene, isolated alkali metal atoms, alkali metal dimers, as well as [alkali metal - pentacene] complexes. We discuss below the pre- and post-photolysis spectra of pentacene isolated in alkali atom-doped matrices.

#### 3.3.1. Pentacene isolated in a Na-doped Ar matrix

##### 3.3.1.a. Pre-photolysis

The mid-IR spectra of co-deposits of alkali metal and pentacene in Ar matrices were also measured and compared to the previous measurements of pentacene isolated in Ar.<sup>19, 21, 48</sup>

Figure 3A displays the mid-IR spectrum ( $1450\text{-}1290\text{ cm}^{-1}$ ) of a co-deposit of Na and pentacene into an Ar matrix. This region has been selected from the entire spectral region scanned ( $5000\text{-}500\text{ cm}^{-1}$ ) as this is the region where the most intense pentacene anion vibrational transitions are found,<sup>19,21</sup> as well as that of the strongest [alkali metal - pentacene] complex spectral features.

Comparison of Figure 3A to that of the spectrum of pentacene isolated in Ar (Figure 3D) reveals that the full absorbance of the most intense features in Figure 3A cannot be due to isolated pentacene. The position of the vibrational band measured at  $1372.6\text{ cm}^{-1}$  closely matches, however, that previously assigned to the most intense spectroscopic feature of the pentacene anion.<sup>19, 21</sup> This previous assignment was based on experiments in which the spectroscopic features of the anion were observed to decrease in intensity upon addition of the electron acceptor  $\text{CCl}_4$  to the matrix while those assigned to the cation increased. If the  $1372.6\text{ cm}^{-1}$  feature does indeed arise from pentacene anions, based upon its measured absorbance, the second most intense feature of the anion at  $1349.2\text{ cm}^{-1}$  should also be observable. This feature, however, is not detected in Figure 3A or is significantly weaker than expected.

Figure 4A displays the near-IR spectrum of the same sample (Na and pentacene in Ar) shown in Figure 3A. The pentacene anion band in Ar, assigned by Szczepanski et al.<sup>19</sup> at  $882.2\text{ nm}$ , is not observed in this spectrum. All spectral features in this spectrum are thus assigned to a [Na - pentacene] complex, as they only appear when both species are present within the matrix, similar to the spectral features noted in Figure 3A. Based upon the absence of the stronger pentacene anion bands in the near-IR shown in Figure 4A and the absence of the second strongest mid-IR anion band discussed above, it is concluded that the vibrational band measured at  $1372.6\text{ cm}^{-1}$  in Figure 3A is not due to the isolated pentacene anion but rather to a [Na - pentacene] complex.

### 3.3.1.b. Post-photolysis

The spectrum of the same matrix used to produce Figure 4A following 4 minutes of photolysis with the high pressure mercury arc lamp is displayed in Figure 4B. The most notable change is the appearance of 3 new, strong, spectral features at  $882.1$ ,  $889.0$ , and  $908.1\text{ nm}$  along

with some weaker features (see Table II). The position of the 882.1 nm feature matches well with that previously assigned to the pentacene anion in Ar at 882.2 nm.<sup>19</sup> We note that all the features seen at wavelengths shorter than 850 nm, and assigned to a [Na - pentacene] complex, are largely unaffected by the photolysis (compare Figures 4A and 4B).

The post-photolysis mid-IR spectrum of the sample used to produce Figure 4B is displayed in Figure 3B. The most notable new feature appears at 1349.2 cm<sup>-1</sup>. The most intense spectral feature at 1321.1 cm<sup>-1</sup> changed only slightly and the feature at 1372.6 cm<sup>-1</sup> grew by ~30%. The intensity ratio between 1372.6 cm<sup>-1</sup> and 1349.2 cm<sup>-1</sup> in Figure 3B is not the expected ratio as produced in the published spectrum of the pentacene anion isolated in an Ar matrix<sup>21</sup> due to the overlap of two spectral absorptions at the 1372.6 cm<sup>-1</sup> position. One is due to the isolated pentacene anion while the other is due to a [Na - pentacene] complex.

### 3.3.2. Pentacene isolated in K-doped Ar and Kr matrices

While the position of the most intense near-IR band at 882.1 nm which appears on photolysis of the pentacene/Na-doped Ar matrix indicates the presence of pentacene anions, the presence of strong spectral features in the mid and near-IR due to the formation of a complex between the Na and pentacene raises the question as to whether the anion produced within the matrix is truly isolated, or whether it involves one or more alkali metals situated in the vicinity of the pentacene molecule. To investigate the nature of the mid and near-IR features and the degree of isolation of the anion, similar experiments were performed in which the alkali metal K was used in place of Na.

Figure 3C displays the mid-IR spectrum of a deposit of K and pentacene in Ar followed by 2 minutes of photolysis by the high pressure mercury arc lamp. The most notable result of changing the alkali metal from Na to K is the appearance of a doublet at 1376.4 and 1372.6 cm<sup>-1</sup>. The spectral positions and intensities of the 1372.6 cm<sup>-1</sup> band and the 1349.2 cm<sup>-1</sup> band is similar to the earlier report for the isolated pentacene anion.<sup>21</sup> The band at 1376.4 cm<sup>-1</sup> in Figure 3C is therefore assigned to a complex between K and pentacene and is probably due to a similar vibrational mode with that which contributed intensity to the band at 1372.6 cm<sup>-1</sup> in Figure 3B.

The mid-IR bands at  $1372.6\text{ cm}^{-1}$  and  $1349.2\text{ cm}^{-1}$  assigned to the *isolated* pentacene anion do not display a measurable shift when using either Na or K as the electron donor in the matrix. The electronic spectrum of the anion, however, may be regarded as a more sensitive measure of the degree of interaction between the alkali metal and the pentacene molecule within the matrix. Figure 4C displays the near-IR spectrum of the same photoionized sample used to produce the spectrum in Figure 3C. While the spectral features seen below 850 nm in Figure 4C have strongly changed in appearance from those observed in Figure 4B, as one would expect for a complex formed between the pentacene molecule and different alkali metals within the matrix, the three intense bands assigned to the pentacene anion do not change in position nor in shape. Based upon these observations, we conclude that the pentacene anions which produce spectral features in the 882-912 nm region are indeed *chemically isolated* from the alkali metal electron donors within the matrix.

Figure 4D displays the near-IR spectrum of a deposit of K and pentacene in Kr followed by 2 minutes of photolysis by the high pressure mercury arc lamp. The experimental parameters used to obtain this spectrum were the same as those used to obtain Figure 4C **except** that the temperature used to vaporize K was lowered from  $130\text{ }^{\circ}\text{C}$  to  $113\text{ }^{\circ}\text{C}$ . As expected from the more polarizable Kr atoms, the spectral features due to the pentacene anion isolated in a Kr matrix have shifted slightly towards the red part of the spectral region as compared with the anion isolated in Ar (see Table II). Comparison of the spectral features attributable to the [K - pentacene] complex isolated in Kr to the equivalent spectral features observed in Ar in Figure 4C suggests that the formation of the [alkali metal - pentacene] complex is, as expected, strongly matrix **dependent**.

### 3.3.3. Pentacene isolated in a Na-doped Ne matrix

The experiments discussed thus far have examined the feasibility of **producing** and detecting isolated pentacene anions within a rare gas matrix. The primary **objective** here is, however, to measure the electronic spectrum of the pentacene ion under conditions **most** relevant to astrophysics (i.e., cold and isolated in the least perturbing environment: a Ne **matrix**). Of additional interest to us is the processes involved in electron transfer during photoionization as well

as while probing the matrix spectroscopically with radiation in the UV. The reported<sup>20</sup> electron affinity of pentacene at 1.35 eV suggests that probing the matrix spectroscopically with radiation of higher energy will result in photodetachment of the electrons from the anions already formed, resulting in the disappearance of the spectral features attributable to anions. The mid and near-IR spectra of the pentacene anion discussed thus far were obtained on the FTIR instrument which, as pointed out in the experimental section, has a red filter implemented on its near-IR source. Only radiation of 665 nm (~1.9 eV) and lower in energy is allowed to irradiate the matrix. Although we have not observed spectral features due to the pentacene anion in the UV/visible spectral regions, the electronic transitions of other PAH anions are expected to extend into this region.<sup>7</sup> This prompted us to explore the effect of increasing the energy of radiation on the yield of pentacene anions, as detected through their strongest electronic absorption transitions.

Figure 5A displays the near-IR spectrum of a [pentacene:Na:Ne] matrix photoionized with the 2.1 eV output of a Na lamp. This radiation is sufficient to photoionize the Na within the matrix.<sup>22,23</sup> This spectrum, along with those displayed in Figures 5B and 5C, has been baseline corrected to remove all spectral contributions of the alkali metal and [alkali metal - pentacene] complex, thus allowing for the clear observation of the less intense features of the isolated pentacene ion. The spectral features observed at 872.6, 883.8, and 904.0 nm are assigned to the isolated pentacene anion in Ne (see Table II). Since the ionization energy of pentacene<sup>49</sup> is 6.61 eV, pentacene cations are not produced here. The same matrix sample was then exposed to the full output of a hydrogen lamp (10.2 eV) and the resulting spectrum is displayed in Figure 5B. The strongest spectral feature due to the pentacene cation is observed to appear (see Table III). The spectrum of the pentacene cation isolated in Ne following irradiation with the Lyman  $\alpha$  line (10.2 eV) is also shown in Figure 5D for reference. The spectral features of the pentacene anion decrease slightly, but do not disappear entirely. Presumably, a dynamic equilibrium exists between the formation of pentacene anions and the photodetachment of the electrons from pentacene anions that have already formed. Thus, both the Lyman  $\alpha$  photolysis radiation and the radiation used to spectroscopically probe the sample to produce Figure 4B have likely neutralized a significant portion of the anions present before photolysis. The photolysis

radiation, however, simultaneously produces additional anions through the process of cationization of neutral pentacene molecules and Na atoms in the matrix.

#### 3.3.4. Pentacene isolated in a K-doped Ne matrix

Figure 5C displays the spectrum resulting after photoionizing a Ne matrix doped with pentacene and K with Lyman  $\alpha$  radiation. As in the case of the sample whose spectrum is displayed in Figure 5B, spectroscopic features due to both pentacene anions and pentacene cations are observed. The position and band shape of all the spectroscopic features do not appear to have been modified by changing from Na to K as the electron donor. Just as in the comparison of Figures 4B and 4C discussed above, the total resemblance of the ionic features in Figures 5B and 5C allows us to conclude that the pentacene anions and cations detected in these spectra are chemically isolated from their counterions within the matrix.

#### 3.4. Assignments of the vibronic features observed for the pentacene cation and anion

The only previous assignment of the electronic absorption spectrum of the pentacene cation is that by Szczepanski et. al.<sup>19</sup> with the use of Ar matrices. In their study, the first two excited states of the cation were observed and assigned based upon gas-phase, photoelectron spectroscopy (PES) measurements.<sup>49</sup> The authors assign the origin of the first excited electronic state ( $D_0$ ) to the most intense spectral feature in their spectra at 954.1 nm. We observe this spectral feature at 943.9 nm in Ne matrices (see Figure 5 and Table III). An alternative possibility would be to assign the band we observe at 979.3 nm in Ne as the  $D_0$  origin. We favor this latter assignment because (i) it takes into account the 3 structures observed at the red of the most intense vibronic transition and (ii) it is in agreement with the expected red-shift of the first electronic state between the gas-phase PES measurement<sup>49</sup> of 946.3 nm and the Ne matrix value. A red-shift from the gas-phase has been systematically observed for all PAH cations examined to date.<sup>24, 25</sup> The spectral feature observed as a shoulder of the vibronic origin in Ar at 990.3 nm is assigned to the pentacene cation trapped in a different site in the matrix. This feature is not observed in Ne

matrices. The origin of the excited electronic state  $D_4$ , assigned by Szczepanski et. al.<sup>19</sup> in Ar at 426.0 nm, is observed in this study at 420.5 nm and 425.1 nm in Ne and Ar, respectively. This is in reasonably good agreement with the gas-phase PES measurement of 445.9 nm.<sup>49</sup>

The assignment of the vibronic features observed for both the cation and anion is made difficult by the lack of information on the vibrational modes of the pentacene ions below 700  $\text{cm}^{-1}$ . The similarity, however, between the separation of the two anion vibronic bands (Table II) with the separation of the second and third vibronic bands of the cation (Table III) gives credence to the assignment of the vibronic origin for the two species. The observed relative intensity of these bands are also comparable. Presumably, this is due to not only the expectation of a close correspondence between the electronic structure of cations and anions of alternate hydrocarbons,<sup>50</sup> but also the expectation of similar molecular geometry for the ions and the neutral molecule.<sup>24, 25</sup> Accordingly, the low-frequency vibronic<sup>51, 52</sup> and vibrational<sup>47, 53, 54</sup> information available in the literature for the neutral pentacene molecule can be used to tentatively assign the vibronic bands of the pentacene cation and anion listed in Tables II and III. We associate the vibronic bands observed below 700  $\text{cm}^{-1}$  for the anion and the cation isolated in neon to modes involving C–C–C out-of-plane bending vibrations. Similarly, the vibronic bands observed at 753  $\text{cm}^{-1}$  and 1807  $\text{cm}^{-1}$  above the  $D_0$  electronic origin for the cation isolated in neon are tentatively assigned to a C–H out-of-plane bending vibration and an overtone or combination band, respectively.

#### 4. SUMMARY AND CONCLUSIONS

In this study, we have reported the first electronic spectrum of the pentacene anion and cation isolated in a Ne matrix where the perturbation is minimal. Co-deposition of pentacene with an alkali metal in a growing rare gas matrix results in vastly improved anion yield relative to photolysis experiments involving pentacene alone within the matrix. The experimental parameters used to obtain and optimize the spectra reported here lead to the observation of spectral features due to five distinct species within the matrix: (i) isolated alkali metal atoms (ii) alkali metal clusters; (iii) isolated neutral pentacene molecules; (iv) neutral alkali metal - pentacene complex(es); and (v) isolated pentacene anions. Experiments performed with K in the place of Na allow one to

disentangle the spectral features of the alkali metal and pentacene complex(es) from those of the isolated pentacene anions while revealing the degree of isolation of the PAH anions which form upon photolysis of the matrix. The results reported here show that *isolated* pentacene anions can indeed be produced within a rare gas matrix that has been doped with an alkali metal.

The results also show that one can spectroscopically probe anions above the electron affinity energy due to a dynamic charge equilibrium within the matrix. This equilibrium is difficult if not impossible to achieve in the gas phase. As it is expected that PAHs other than pentacene also form anions, it is planned to continue these experiments involving the use of alkali metal doped matrices to optimize the in-situ production of negatively-charged PAHs.

## ACKNOWLEDGMENTS

The authors thank R. Walker for his invaluable expert assistance in developing the experimental apparatus. T. M. H. would also like to acknowledge the support of the National Research Council in the form of an associateship. This research was supported by NASA's Office of Space Science (Grant No. 344-01-57-41).

## REFERENCES

- <sup>1</sup>P. Swings and L. Rosenfeld, *Astrophys. J.* **86**, 483 (1937).
- <sup>2</sup>M. B. Bell, P. A. Feldman, M. J. Travers, M. C. McCarthy, C. A. Gottlieb and P. Thaddeus, *Astrophys. J. Lett.* **483**, L61 (1997).
- <sup>3</sup>D. Smith and P. Spanel, *Mass Spectrom. Rev.* **14**, 255 (1995).
- <sup>4</sup>L. J. Allamandola, A. G. G. M. Tielens, and J. R. Barker, *Astrophys. J. Suppl. Ser.* **71**, 733 (1989).
- <sup>5</sup>J. L. Puget and A. Léger, *Annu. Rev. Astron. Astrophys.* **27**, 161 (1989).
- <sup>6</sup>D. M. Hudgins and L. J. Allamandola, *Astrophys. J. Lett.* **513**, L69 (1999).
- <sup>7</sup>F. Salama, E. L. O. Bakes, L. J. Allamandola, and A. G. G. Tielens, *Astrophys. J.* **458**, 621 (1996).
- <sup>8</sup>F. Salama, G. A. Galazutdinov, J. Krelowski, L. J. Allamandola, and F. A. Musaev, *Astrophys. J.* in press (1999).
- <sup>9</sup>A. Omont, *Astron. Astrophys.* **164**, 159 (1986).

- <sup>10</sup>S. Lepp and A. Dalgarno, *Astrophys. J.* **324**, 553 (1988).
- <sup>11</sup>S. Lepp and A. Dalgarno, *Astrophys. J.* **335**, 769 (1988).
- <sup>12</sup>A. G. G. M. Tielens, in *Dust and Chemistry in Astronomy*, edited by T. J. Millar and D. A. Williams (IOP Pub., Bristol, 1993), pp. 103-141.
- <sup>13</sup>E. Dartois and L. d'Hendecourt, *Astron. Astrophys.* **323**, 534 (1997).
- <sup>14</sup>E. L. O. Bakes and A. G. G. M. Tielens, *Astrophys. J.* **499**, 258 (1998).
- <sup>15</sup>T. J. Lee and C. E. Dateo, *Spectrochim. Acta* **55A**, 739 (1999).
- <sup>16</sup>T. Shida and S. Iwata, *J. Am. Chem. Soc.* **95**, 3473 (1973).
- <sup>17</sup>T. Shida, *Electronic Absorption Spectra of Radical Ions* (Elsevier, Amsterdam, 1988).
- <sup>18</sup>T. Henning and F. Salama, *Science* **282**, 2204 (1998).
- <sup>19</sup>J. Szczepanski, C. Wehlburg, and M. Vala, *Chem. Phys. Lett.* **232**, 221 (1995).
- <sup>20</sup>L. Crocker, T. Wang, and P. Kebarle, *J. Am. Chem. Soc.* **115**, 7818 (1993).
- <sup>21</sup>D. M. Hudgins and L. J. Allamandola, *J. Phys. Chem.* **99**, 8978 (1995).
- <sup>22</sup>P. H. Kasai, *Acc. Chem. Res.* **4**, 329 (1971).
- <sup>23</sup>R. Köppe and P. H. Kasai, *J. Phys. Chem.* **98**, 12904 (1994).
- <sup>24</sup>F. Salama and L. J. Allamandola, *J. Chem. Phys.* **94**, 6964 (1991).
- <sup>25</sup>F. Salama, C. Joblin, and L. J. Allamandola, *J. Chem. Phys.* **101**, 10252 (1994).
- <sup>26</sup>D. M. Hudgins, S. A. Sanford, and L. J. Allamandola, *J. Phys. Chem.* **98**, 4243 (1994).
- <sup>27</sup>D. M. Hudgins and L. J. Allamandola, *J. Phys. Chem.* **99**, 3033 (1995).
- <sup>28</sup>L. C. Balling, M. D. Havey, and J. F. Dawson, *J. Chem. Phys.* **69**, 1670 (1978).
- <sup>29</sup>J. Hormes and B. Karrasch, *Chem. Phys.* **70**, 29 (1982).
- <sup>30</sup>L. C. Balling and J. J. Wright, *J. Chem. Phys.* **81**, 675 (1984).
- <sup>31</sup>S. Tam and M. E. Fajardo, *J. Chem. Phys.* **99**, 854 (1993).
- <sup>32</sup>J. A. Boatz and M. E. Fajardo, *J. Chem. Phys.* **101**, 3472 (1994).
- <sup>33</sup>D. C. Silverman and M. E. Fajardo, *J. Chem. Phys.* **106**, 8964 (1997).
- <sup>34</sup>M. Groß and F. Spiegelmann, *J. Chem. Phys.* **108**, 4148 (1998).
- <sup>35</sup>J. J. Wright and L. C. Balling, *J. Chem. Phys.* **73**, 994 (1980).
- <sup>36</sup>H. Coufal and E. Lüscher, *Phys. Lett.* **48A**, 445 (1974).
- <sup>37</sup>H. Coufal, U. Nagel, M. Burger, and E. Lüscher, *Z. Phys. B* **25**, 227 (1976).

- <sup>38</sup>H. Coufal, U. Nagel, and E. Lüscher, *Ber. Bunsenges. Phys. Chem.* **82**, 133 (1978).
- <sup>39</sup>L. C. Balling, M. D. Havey, and J. J. Wright, *J. Chem. Phys.* **70**, 2404 (1979).
- <sup>40</sup>H. Kuppelmaier, H.-J. Stöckmann, A. Steinmetz, E. Görlach, and H. Ackermann, *Phys. Lett.* **98A**, 187 (1983).
- <sup>41</sup>A. Schrimpf, G. Sulzer, H.-J. Stöckmann, and H. Ackermann, *Phys. Lett.* **110A**, 327 (1985).
- <sup>42</sup>A. Steinmetz, A. Schrimpf, H.-J. Stöckmann, E. Görlach, R. Dersch, G. Sulzer, and H. Ackermann, *Z. Phys. D* **4**, 373 (1987).
- <sup>43</sup>A. Schrimpf, G. Sulzer, H.-J. Stöckmann, and H. Ackermann, *Z. Phys. B* **67**, 531 (1987).
- <sup>44</sup>H. B. Klevens and J. R. Platt, *J. Chem. Phys.* **17**, 470 (1949).
- <sup>45</sup>T. E. Orlowski and A. H. Zewail, *J. Chem. Phys.* **70**, 1390 (1979).
- <sup>46</sup>E. Heinecke, D. Hartmann, R. Müller, and A. Hese, *J. Chem. Phys.* **109**, 906 (1998).
- <sup>47</sup>L. Colangelli, V. Mennella, G. A. Baratta, E. Bussoletti, and G. Strazzulla, *Astrophys. J.* **396**, 369 (1992).
- <sup>48</sup>D. M. Hudgins and S. A. Sandford, *J. Phys. Chem.* **102**, 344 (1998).
- <sup>49</sup>W. Schmidt, *J. Chem. Phys.* **66**, 828 (1977).
- <sup>50</sup>A. D. McLachlan, *Mol. Phys.* **2**, 271 (1959).
- <sup>51</sup>A. Amirav, U. Even, and J. Jortner, *Chem. Phys. Lett.* **72**, 21 (1980).
- <sup>52</sup>A. M. Griffiths and P. A. Freedman, *J. Chem. Soc., Faraday Trans. 2*, **78**, 391 (1982).
- <sup>53</sup>K. Ohno, *J. Mol. Spectrosc.* **77**, 329 (1979).
- <sup>54</sup>S. J. Cyvin, G. Neerland, B. N. Cyvin, and J. Brunvoll, *J. Mol. Spectrosc.* **83**, 471 (1980).

Figure 1. The visible/near-IR spectra of a co-deposit of (A) Na in Ar; (B) Na in Ne; (C) K in Ar; (D) K in Ne; and (E) pentacene and Na in Ne. The spectrum displayed in (E) corresponds to a 4 hr deposition while the others were taken from 2 hr depositions. The gas-phase spectral positions of the D lines of Na and K are displayed as vertical lines on the bottom of the plot. The doublet D lines of Na are not resolvable with the scale used for this plot.

Figure 2. The UV/visible spectra of a co-deposit of (A) pentacene in Ne; (B) pentacene in Ar; and (C) pentacene in Kr. Each complete spectrum was taken after a 5 min deposition. The inset spectra were taken after 2 hr depositions to enhance the weaker spectral features.

Figure 3. The mid-IR spectra of (A) a 2 hr deposit of Na and pentacene in Ar; (B) the same sample after 4 min of high pressure mercury lamp photolysis; (C) a 2 hr deposit of K and pentacene in Ar followed by 2 minutes of mercury arc lamp photolysis; and (D) a 3 hr deposit of pentacene in Ar.

Figure 4. The near-IR spectra of (A) a 2 hr deposit of Na and pentacene in Ar; (B) the same sample after 4 min of high pressure mercury lamp photolysis; (C) a 2 hr deposit of K and pentacene in Ar followed by 2 minutes of mercury arc lamp photolysis; and (D) a 2 hr deposit of K and pentacene in Kr followed by 2 minutes of mercury arc lamp photolysis.

Figure 5. The near-IR spectra of (A) a 2 hr deposit of Na and pentacene in Ne followed by 20 minutes of Na lamp photolysis; (B) the same sample after an additional 20 minutes of Lyman  $\alpha$  photolysis; (C) a 2 hr deposit of K and pentacene in Ne followed by 10 minutes of Lyman  $\alpha$  photolysis; and (D) a 2 hr deposit of pentacene in Ne followed by 10 minutes of Lyman  $\alpha$  photolysis. The pre-photolysis spectrum in each case was used as the background for the resulting spectrum. The spectra shown in (A), (B), and (C) were baseline corrected to remove the broad underlying absorption due to the alkali metal and the [alkali metal - pentacene] complex shown in Figure 1E.

Table I. Vibronic transitions of neutral pentacene isolated in Ne, Ar, and Kr matrices shown in Figure 2.

Table II. Vibronic transitions of the pentacene anion isolated in Ne, Ar, and Kr matrices shown in Figures 4 and 5.

Table III. Vibronic transitions of the pentacene cation isolated in Ne, Ar, and Kr matrices.

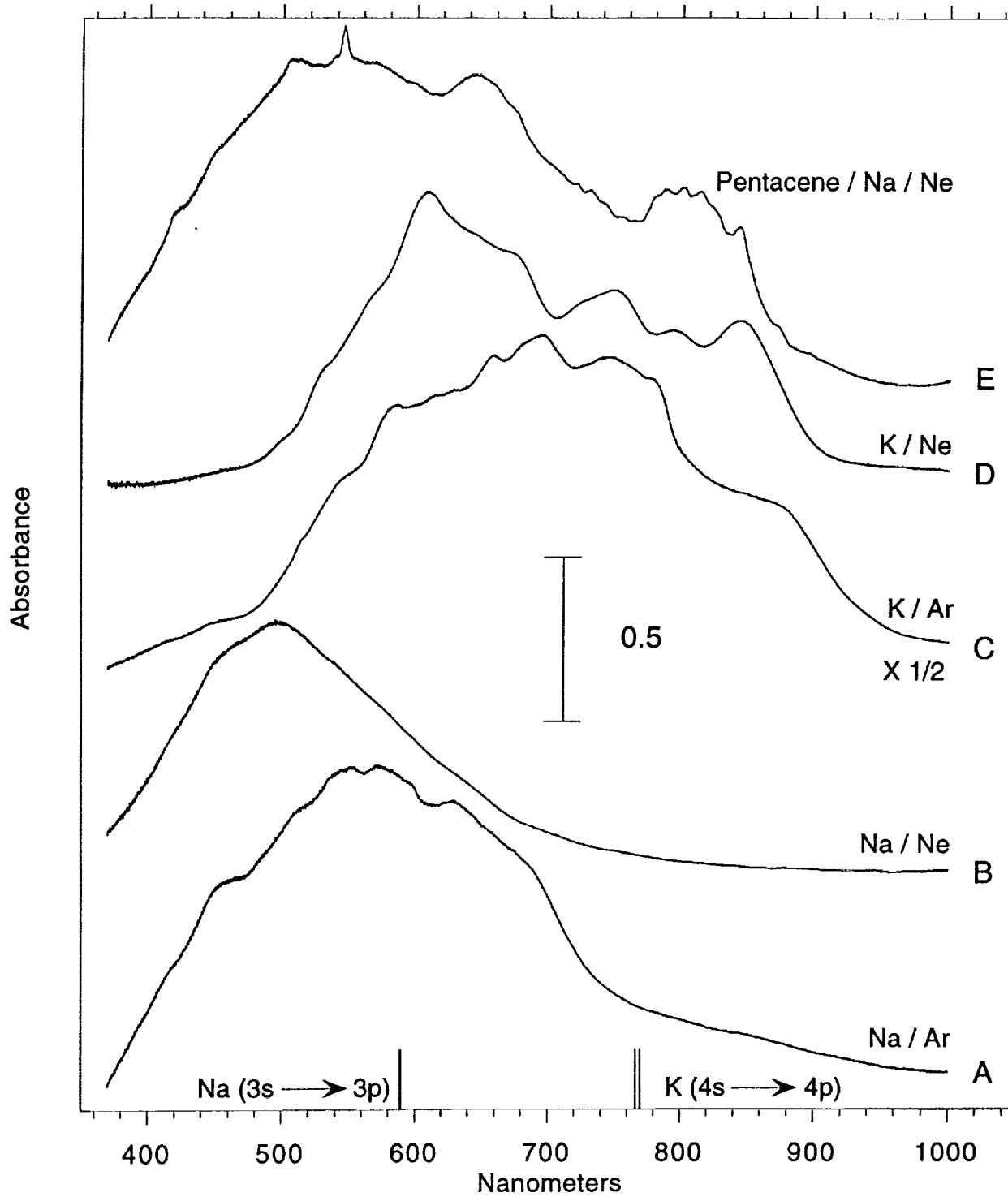


Figure 1

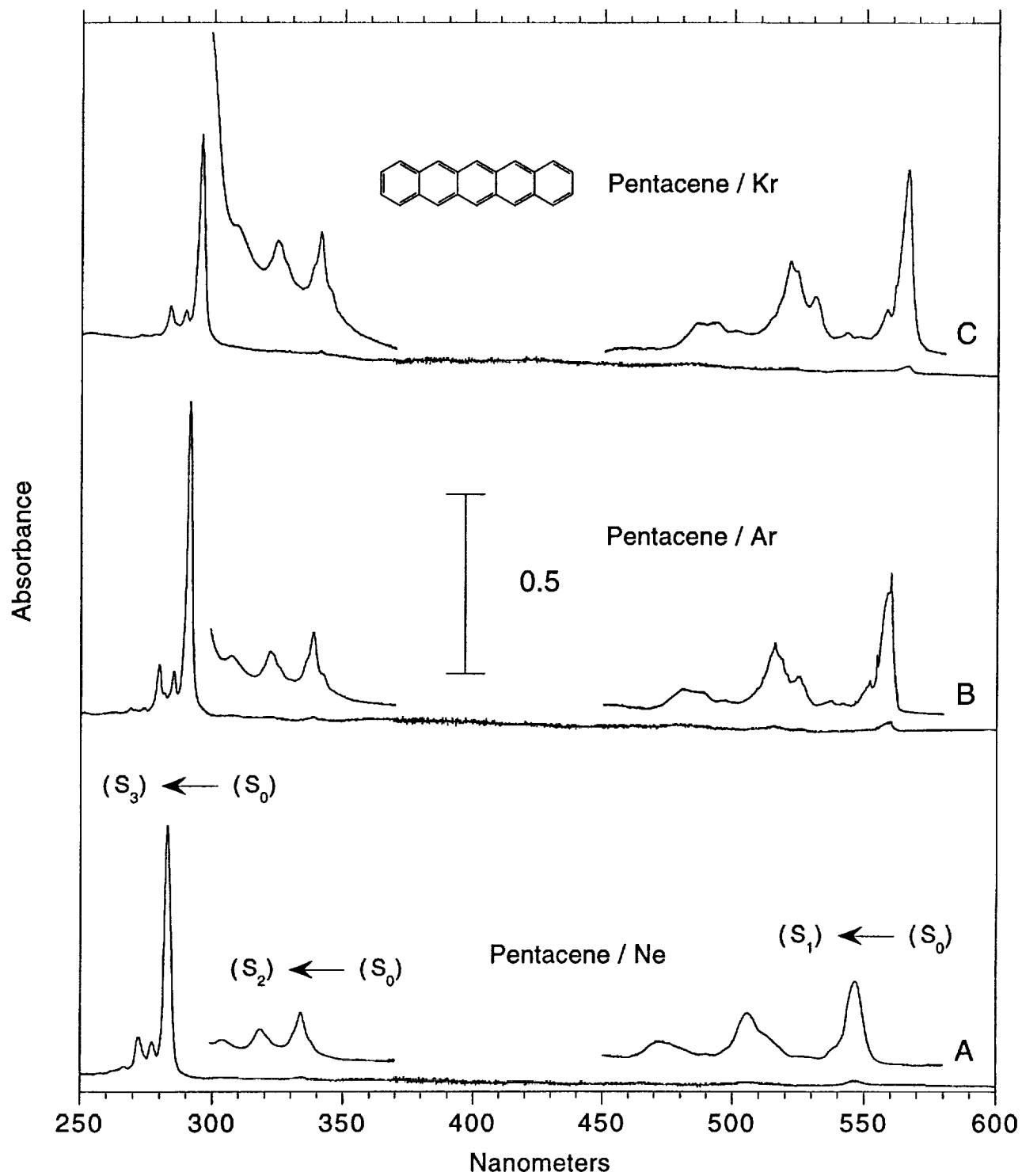


Figure 2

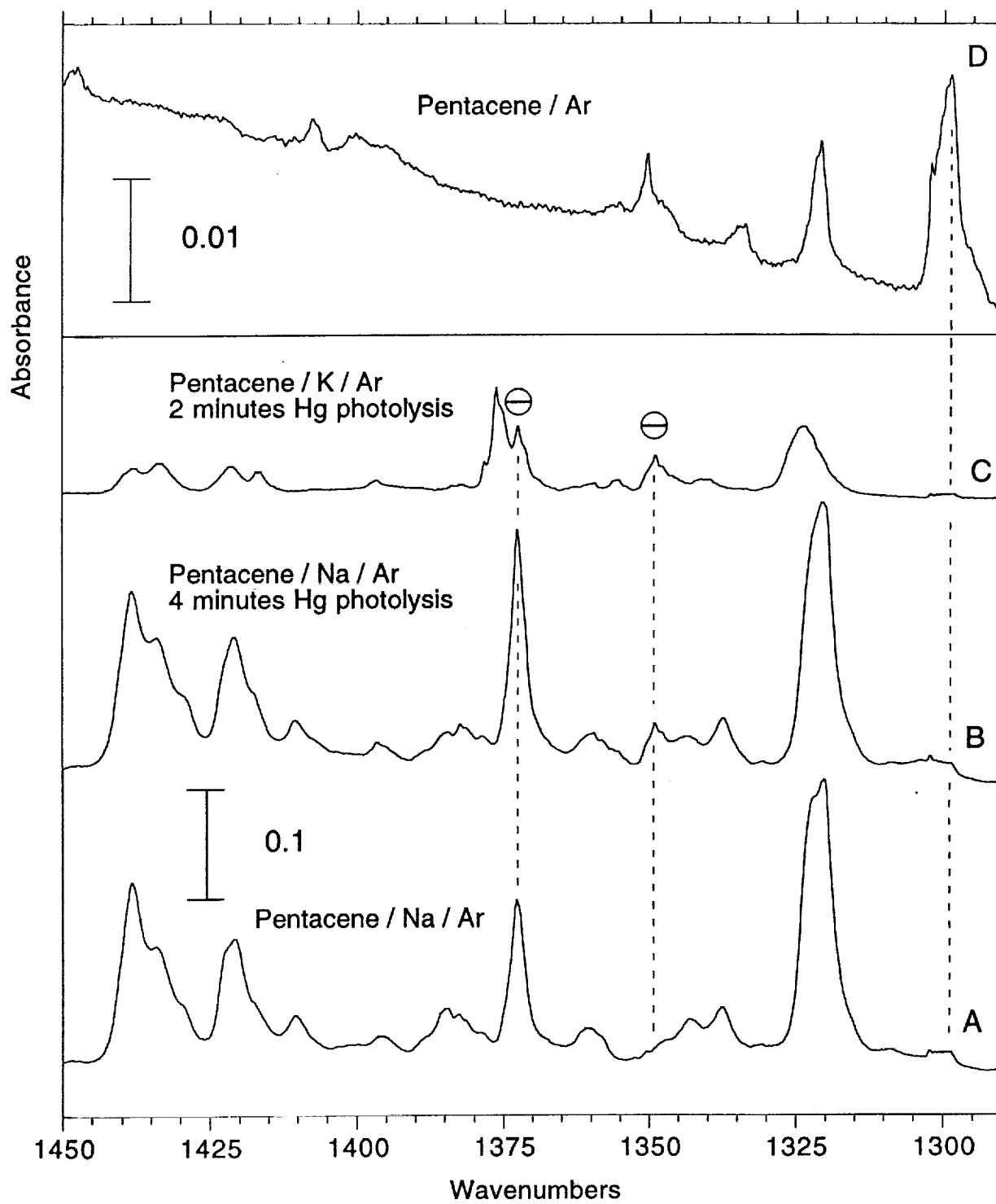


Figure 3

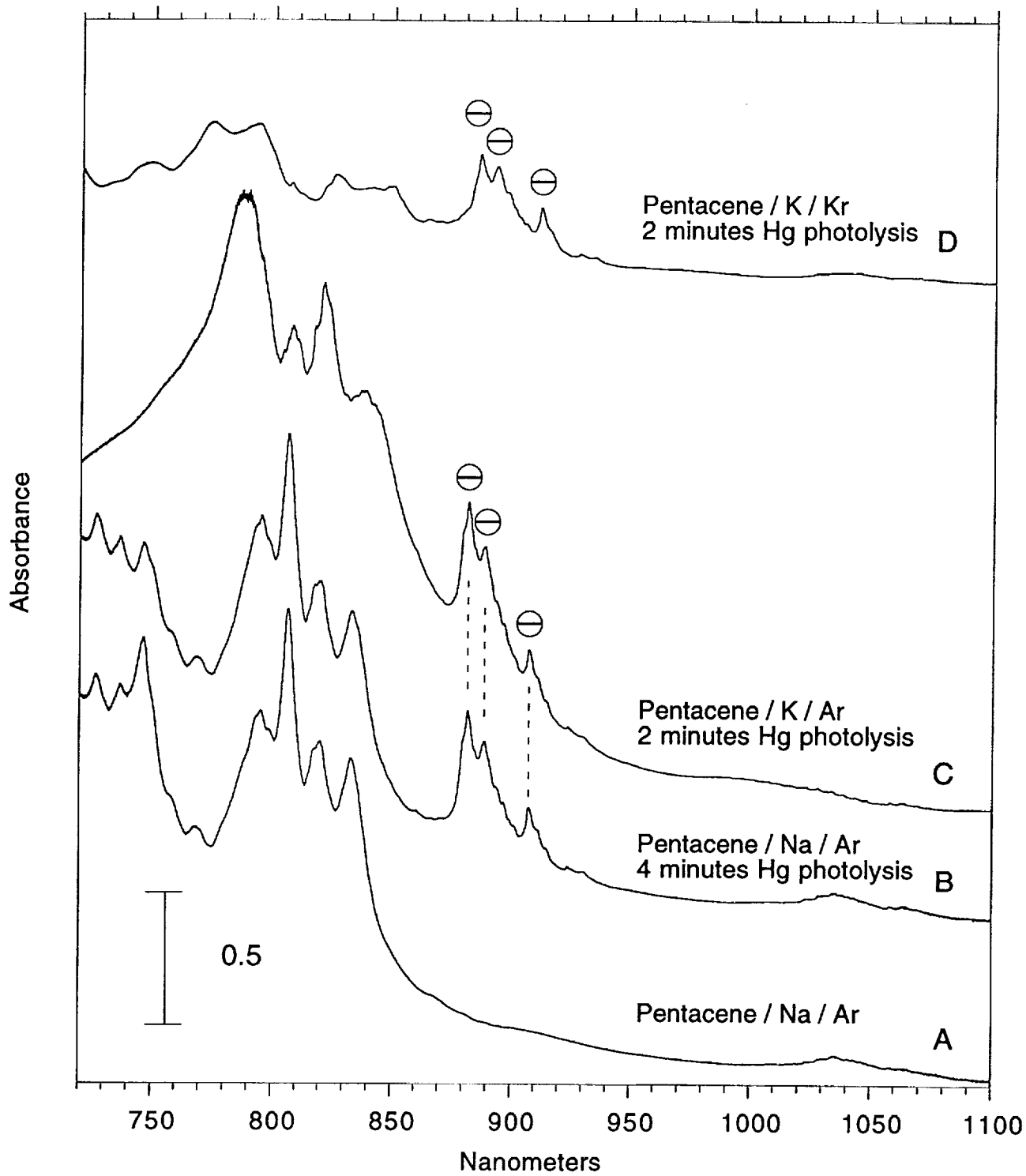


Figure 4

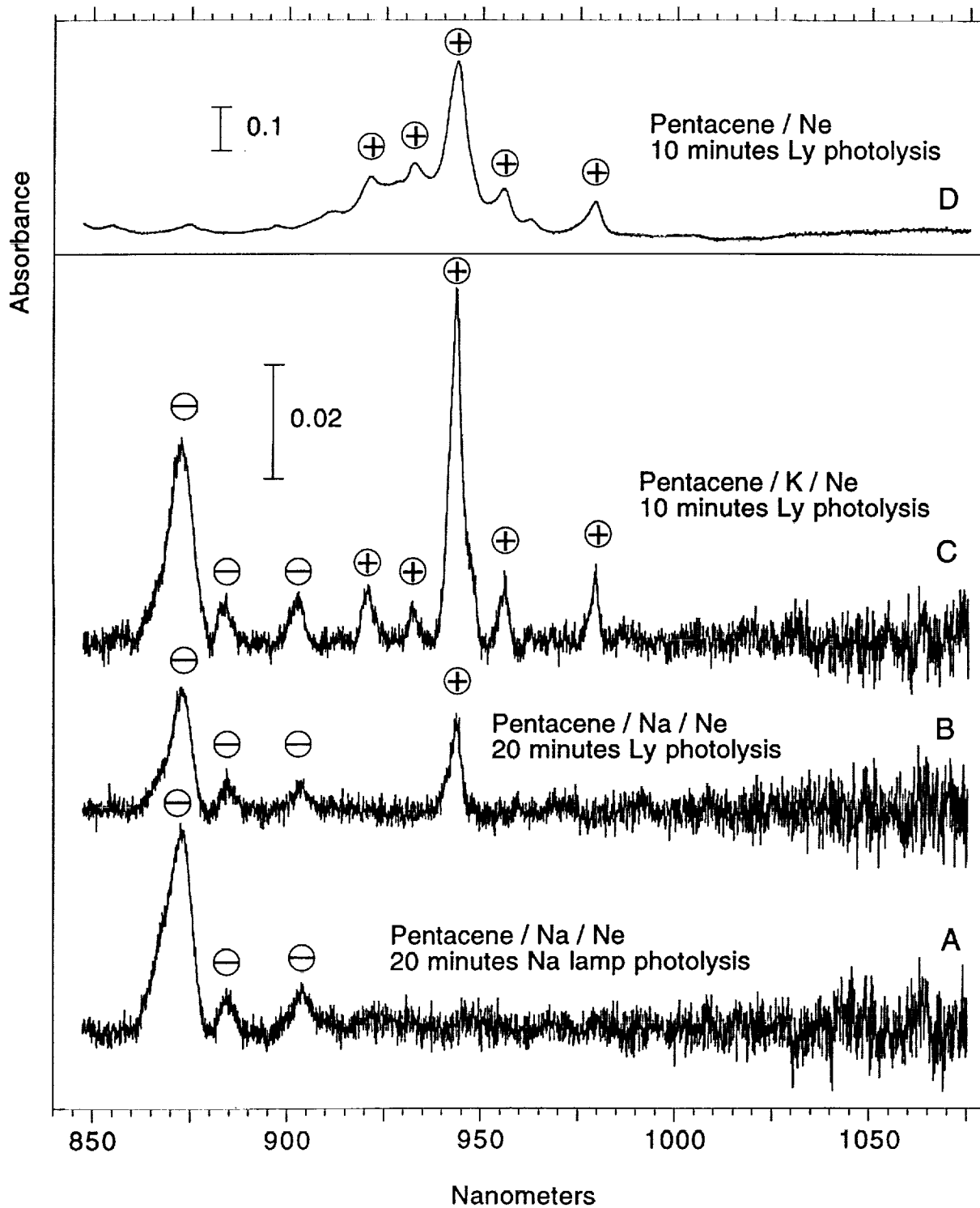


Figure 5

Assignment	Ne		Ar		Kr		Rel. Shift	
	$\lambda$ (nm)	$\nu$ (cm <sup>-1</sup> )	$\lambda$ (nm) <sup>b</sup>	$\nu$ (cm <sup>-1</sup> )	$\lambda$ (nm)	$\nu$ (cm <sup>-1</sup> )	$\nu_{(Ne-Kr)} / \nu_{Ne}$ (%)	$\nu_{(Ne-Kr)} / \nu_{Ne}$ (%)
$\nu_{CC}$ stretch	270.7	36 941	279.6	35 765	283.5	35 273	3.2	4.5
$\nu_{CH}$    bend	275.8	36 258	285.1	35 075	289.3	34 566	3.3	4.7
${}^1B_{3u}(S_2) \leftarrow {}^1A_{1g}(S_0)$	281.5 <sup>a</sup>	35 524	291.2 <sup>a</sup>	34 341	295.5 <sup>a</sup>	33 841	3.3	4.7
$\nu_{CH}$ stretch; $2\nu_{CC}$ stretch	303.2	32 982	306.9	32 584	308.9	32 373	1.2	1.8
$\nu_{CC}$ stretch	317.4	31 506	322.1	31 046	324.4	30 826	1.5	2.2
${}^1B_{3u}(S_2) \leftarrow {}^1A_{1g}(S_0)$	332.9 <sup>a</sup>	30 039	338.4 <sup>a</sup>	29 551	340.9 <sup>a</sup>	29 334	1.6	2.3
$2\nu_{CC}$ stretch	471.1	21 227	480.4	20 816	487.5	20 513	1.9	3.4
			(480.2)	(20 825)				
	---	---	488.2	20 483	492.8	20 292	---	---
$\nu_{CC}$ stretch	504.5	19 822	515.8	19 387	521.4	19 179	2.2	3.2
			(515.6)	(19 395)				
$\nu_{CH \perp}$ bend	510.8	19 577	524.7	19 059	530.7	18 843	2.6	3.7
${}^1B_{3u}(S_1) \leftarrow {}^1A_{1g}(S_0)$	544.4 <sup>a</sup>	18 369	559.8 <sup>a</sup>	17 864	566.0 <sup>a</sup>	17 668	2.8	3.8
			(559.7)	(17 867)				

a. Strongest band of the system.

b. Values in parentheses are taken from reference 19.

Table I

Assignment	Ne		Ar		Rel. Shift		Kr		Rel. Shift	
	$\lambda$ (nm)	$\nu$ ( $\text{cm}^{-1}$ )	$\lambda$ (nm) <sup>b</sup>	$\nu$ ( $\text{cm}^{-1}$ )	$\nu$ ( $\text{cm}^{-1}$ )	$\nu_{(\text{Ne-Ar})} / \nu_{\text{Ne}}$ (%)	$\lambda$ (nm)	$\nu$ ( $\text{cm}^{-1}$ )		$\nu$ ( $\text{cm}^{-1}$ )
	872.6 <sup>a</sup>	11 460	882.1 <sup>a</sup>	11 337	325	1.1	886.4 <sup>a</sup>	11 282	312	1.6
			(882.2)	(11 335)						
	883.8	11 315	889.0	11 249	237	0.6	893.1	11 197	227	1.0
(D <sub>1</sub> ) ← (D <sub>0</sub> )	904.0	11 062	908.1	11 012	0	0.5	911.6	10 970	0	0.8

a. Strongest band of the system.

b. Values in parentheses are taken from reference 19.

Table II

Assignment	Ne		Ar		Kr		Rel. Shift $v_{(Ne-Kr)} / v_{Ne}$ (%)
	$\lambda$ (nm)	$\nu$ (cm <sup>-1</sup> )	$\lambda$ (nm) <sup>b</sup>	$\nu$ (cm <sup>-1</sup> )	$\lambda$ (nm)	$\nu$ (cm <sup>-1</sup> )	
<sup>3</sup> B <sub>u</sub> (D <sub>1</sub> ) ← <sup>3</sup> B <sub>g</sub> (D <sub>0</sub> )	420.5 <sup>a</sup>	23 781	425.1 <sup>a</sup> (426.0)	23 524 (23 474)	0	0	1.1
	832.1	12 018	842.3 (842.2)	11 872 (11 874)	1724	11 822	1.2
	912.1	10 964	931.6 (931.7)	10 734 (10 733)	586	10 691	2.1
	921.5	10 852	938.9 (940.3)	10 651 (10 635)	503	10 615	1.9
	933.6	10 711	947.4 (947.8)	10 555 (10 551)	407	10 498	1.5
	943.9 <sup>a</sup>	10 594	955.0 <sup>a</sup> (954.1)	10 471 (10 481)	323	10 428	1.2
	955.7	10 464	962.1 (961.9)	10 394 (10 396)	246	10 357	0.7
	962.8	10 386	968.6 (968.5)	10 324 (10 325)	176	10 311	0.6
	979.3	10 211	985.4 (984.9)	10 148 (10 153)	0	10 121	0.6
	matrix site	----	----	990.3 (990.6)	10 098 (10 095)	----	----
<sup>2</sup> A <sub>u</sub> (D <sub>1</sub> ) ← <sup>2</sup> B <sub>g</sub> (D <sub>0</sub> )	420.5 <sup>a</sup>	23 781	425.1 <sup>a</sup> (426.0)	23 524 (23 474)	0	0	1.1
	832.1	12 018	842.3 (842.2)	11 872 (11 874)	1724	11 822	1.2
	912.1	10 964	931.6 (931.7)	10 734 (10 733)	586	10 691	2.1
	921.5	10 852	938.9 (940.3)	10 651 (10 635)	503	10 615	1.9
	933.6	10 711	947.4 (947.8)	10 555 (10 551)	407	10 498	1.5
	943.9 <sup>a</sup>	10 594	955.0 <sup>a</sup> (954.1)	10 471 (10 481)	323	10 428	1.2
	955.7	10 464	962.1 (961.9)	10 394 (10 396)	246	10 357	0.7
	962.8	10 386	968.6 (968.5)	10 324 (10 325)	176	10 311	0.6
	979.3	10 211	985.4 (984.9)	10 148 (10 153)	0	10 121	0.6
	matrix site	----	----	990.3 (990.6)	10 098 (10 095)	----	----

a. Strongest band of the system.

b. Values in parentheses are taken from reference 19.

Table III

